Adsorption
https://doi.org/10.1007/s10450-019-00098-2

Carbon/montmorillonite hybrids with different activation methods: adsorption of norfloxacin

María Emilia Zelaya Soulé[1] · Facundo Barraqué[1] · Federico Manuel Flores[1] · Rosa M. Torres Sánchez[1] · Mariela A. Fernández[1]

Received: 29 June 2018 / Revised: 12 February 2019 / Accepted: 22 April 2019

Abstract
Within the group of emerging pollutants, antibiotics have raised scientific concern due to, among others, their negative influence on the health of living beings. To investigate the adsorption capacity of the antibiotic norfloxacin (NFX), in this work carbon/montmorillonite hybrid materials (MD) obtained by hydrothermal synthesis using dextrose as carbon source, with acid and thermal activation methods, as well as some precursor materials, were deeply characterized. The characterization results of MD showed the presence of carbon at both the interlayer and external surfaces of montmorillonite (M), with an increase of more than three times in the specific surface area and also in the negative surface electrical charge with respect to M sample. The MD materials assayed were effective (around 40%) to remove NFX from aqueous medium at pH 7, the removal efficiency being within that of the M (75–99%) and hydrothermal carbon (5%) samples. The XRD and zeta potential values of NFX adsorbed products indicated that, while in M sample the interlayer is the preferential adsorbing surface, for the MD material assayed (activated with higher acid concentration) the external surface would be the more active.

Keywords Hydrothermal carbon · Montmorillonite · Activation · Norfloxacin · Adsorption

1 Introduction

In the last years, a new kind of pollutants, called emerging pollutants, has been detected in wastewater (e.g., surfactants, pharmaceutical compounds, hormones, illicit drugs) (Ania et al. 2011). The efficient removal of emerging pollutants from wastewater, particularly antibiotics, is of great importance because they not only affect aquatic life, but also favor bacterial resistance causing many detrimental effects on the environment and human health (Kerkez-Kuyumcu et al. 2016).

Norfloxacin (NFX), an antibiotic of the fluoroquinolone family, is widely used against Gram-negative and Gram-positive bacteria (Liu et al. 2011). The NFX has a zwitterion form, with two pKa (6.22 and 8.51), due to the presence of two proton-binding sites (carboxyl and amine groups, respectively). It exists either in NFX^+, $NFX^{\pm}$ or NFX^- form in aqueous solution at $6.22 \leq pH \leq 8.51$, (Pei et al. 2012). The amounts of unchanged NFX excreted in urine (48 h period) were found to be 24% (Zeiler et al. 1988), reaching the environment through municipal, hospital and industrial wastewater effluents (Özcan et al. 2016). For example, an average NFX concentration of 1.3×10^{-6} mM was found in wastewater treatment plants in USA (Fu et al. 2017), while 0.02×10^{-3} mM was reported in Bohai Bay, China (Bu et al. 2013). Some water treatment technologies such as activated sludge (Zorita et al. 2009), biological degradation (Martínez-Alcalá et al. 2017) and photocatalytic decomposition (Sturini et al. 2012) have proved to be ineffective to remove NFX, the adsorption method remaining as one attractive remediation option.

Due to its high specific surface, microporous nature and excellent adsorption capacity, commercial activated carbon is often used as an adsorbent widely applied in wastewater treatment (Wu et al. 2011). However, the relatively high cost has limited its use, and its replacement with materials obtained from biomass has been presented as an alternative

Electronic supplementary material The online version of this article (https://doi.org/10.1007/s10450-019-00098-2) contains supplementary material, which is available to authorized users.

✉ Mariela A. Fernández
marielafernandez0712@gmail.com

[1] Centro de Tecnología de Recursos Minerales y Cerámica, CETMIC, CIC-CONICET CCT-La Plata, Camino Centenario y 506, M.B. Gonnet, Argentina

Published online: 30 April 2019

option for water treatment (Paredes-Laverde et al. 2018). In the last years, a new adsorbent product coming from hydrothermal carbonization (HTC) of water soluble carbohydrates has emerged, in which the oxygen-containing groups anchored on the surface are the main adsorbent groups involved (Ai and Li 2013; Makowski et al. 2008; Mochidzuki et al. 2005; Skubiszewska-Zięba et al. 2011). However, HTC materials do not develop large specific surfaces, which has limited their use as adsorbents (Kubo et al. 2010; Yao et al. 2014; Zhang et al. 2015; Zhu et al. 2014). Different activation methods have been proposed to increase the HTC material surface area, phosphoric acid activation with further thermal treatment being one of the most successful (Puziy et al. 2003). In addition to its low cost and the fact of being more environmentally friendly than alkaline hydroxides, this activation process could also raise the possibility of the adsorbent recovery after its use (Wang et al. 2011).

Moreover, clay minerals and particularly montmorillonite (M) have also been proven to be important adsorbents. In addition to its low toxicity and cost, M presents a high specific surface area (Gamba et al. 2017), which can also be improved by acid treatment (Wang et al. 2010a) to increase the amount of molecules and ions retained from the aqueous solution (Bhattacharyya and Gupta 2008; Lin et al. 2004; Torres Sánchez et al. 2011).

However, M technological application is limited by its great swelling property (Low 1980) and low coagulation. It is of interest to obtain and study the characteristics of modified M with the aim of improving some of its technological properties. One of the modifications that can be made consists of obtaining HTC materials in the presence of M, resulting in a hybrid material that can present new and interesting adsorption properties. The swelling of the raw montmorillonite and the consequent decrease in permeability, which limits its use in columns, could be surpassed by these hybrid materials, allowing its technological application. Dextrose (D) has been one of the most used carbohydrates employed (Li et al. 2014).

Particularly, NFX adsorption on K^+ exchanged M has been proven to be pH independent between 4.0 and 8.0 due to the NFX zwitterion characteristics (Pei et al. 2012), and also optimal NFX adsorption has been obtained at pH 7.0 in carbon from lingo-cellulosic biomass (Yan et al. 2017).

In this study, D was selected as carbon former in the M-D hybrid material (MD), which was obtained by hydrothermal carbonization. A deep characterization of initial materials and products has been performed by N_2 and water vapor adsorption measurements, X-ray diffraction (XRD) and zeta potential determinations. The products obtained, as well as raw M and HTC material without M, were used to compare NFX removal efficiency. Besides, NFX adsorption on selected MD materials was carried out to investigate their NFX removal ability from aqueous solutions, and the surface sites involved in the adsorption process were evaluated to determine their feasibility as novel adsorbents in environmental remediation.

2 Materials and methods

2.1 Materials

Na-montmorillonite (> 99%) coming from the Lago Pellegrini deposit, Río Negro, North Patagonia, Argentina, was provided by Castiglioni Pes y Cia, used as received and labelled M. The structural formula obtained from the chemical analysis was $\left[\left(Si_{3.89}Al_{0.11}\right)\left(Al_{1.43}Fe^{3+}_{0.28}Mg_{0.30}\right)O_{10}(OH)_2\right]Na^+_{0.41}$, and its main properties were: isoelectric point (IEP) pH 2.7, total specific surface area (TSSA) = 621 $m^2\ g^{-1}$, and cationic exchange capacity (CEC) = 0.825 mmol g^{-1} (Gamba et al. 2015).

Dextrose (D), MW 180 g mol^{-1} and melting point at 146 °C, was from Anedra. NFX, (1-ethyl-6-fluoro-1,4-dihydro-4-oxo-7-(1-piperazinyl)-3-quinolinecarboxylic acid), MW 319.33 g mol^{-1}, solubility in water 0.39 g L^{-1}(Loh et al. 2014), pKa at 6.2 and 8.5 (Li et al. 2017), corresponding to carboxylic and protonated amine group formation, respectively, and isoelectric point at pH 7.4 (Ross and Riley 1990) was provided by Parafarm, and H_3PO_4 (85%) was purchased from Lab. Cicarelli. All chemicals were of analytical grade and used as received without further purification.

Figure 1 shows the structure scheme of NFX.

2.2 Methods

2.2.1 Carbon synthesis by hydrothermal carbonization

A montmorillonite suspension of 10 g L^{-1} in deionized water (Milli-Q) was sonicated for 3 h. Then a 10 g L^{-1} solution of D was added, sonicated for 10 min and identified as MD. To attain an in situ activation, in indicated dispersions, 0.16

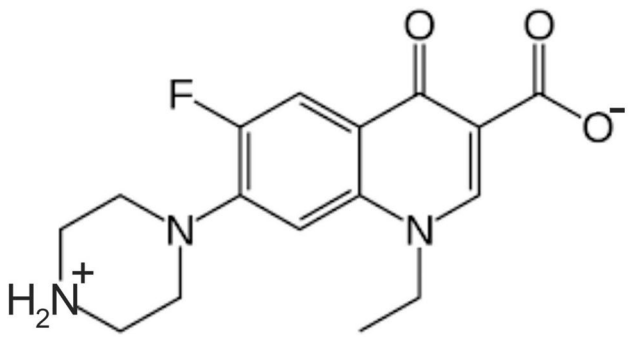

Fig. 1 Structure scheme of NFX

or 0.50% V/V of H_3PO_4, named ac1 and ac3, respectively, was incorporated. The dispersions obtained were placed in a Teflon-lined autoclave, and heated at 210 °C for 24 h. The solid products were filtered and washed with ethanol: water (1:3), dried at 60 °C overnight and ground into powder. Some amounts of these products were post-activated by thermal treatment at 500 °C for 1 h, in a N_2 atmosphere oven. Also a 10 g L^{-1} solution of dextrose sonicated for 10 min and treated at 210 °C for 24 h (D-210) and M thermally treated at 210 °C for 24 h and then at 500 °C for 1 h (M-210 and M-210-500) were obtained for further characterization. Applied treatments and the obtained products are summarized in Table 1.

2.2.2 Sample characterization

Nitrogen adsorption–desorption isotherms were measured by nitrogen adsorption (S_{N2}) at − 196 °C, previously dried at 130 °C for 6 h under high vacuum, using a Micromeritics Accusorb 2100 E instrument.

Water vapor adsorption was determined at room temperature and relative humidity of 47% and was calculated following the procedure indicated in previous work (Torres Sánchez et al. 2011).

The apparent particle diameter determination was performed in Brookhaven 90Plus/Bi-MAS equipment on 1 g L^{-1} sample suspension in KCl 10^{-3} M, employing multi-angle function particle sizing function and dynamic light scattering (DLS). The equipment operated at: $\lambda = 635$ nm; 15 mW solid state laser; scattering angle = 90° and temperature = 25 °C. The determination reproduced the apparent particle diameter of equivalent sphere, Dapp.

Contact angle (CA) measurements were performed using the sessile drop method (Del Mar Orta et al. 2019) on pressed samples (34.3 MPa), in order to evaluate the wettability properties of some samples (Metya et al. 2014; Peng and Yang 2017). Briefly, a drop of deionized water (V = 10 µL) was placed on the sample and after 30 ms, when mechanical perturbations had ended, the CA was measured using the photographic camera of the Linseis L74PT1600 thermal microscope at room temperature. The images were analyzed with a plugin described in previous work (Stalder et al. 2010) and with the open-source software ImageJ V. 1.46r (Rasband 1997).

Powder samples were X-rayed within $3° < 2\theta < 70°$, using a Bruker diffractometer with counting time of 1 s $step^{-1}$, 0.040° (2θ) step size, 40 kV and 35 mA with CuK_α radiation. In addition, samples with NFX adsorbed were scanned in an oriented mode in order to improve the precision of the peak values (Pacuła et al. 2006). These samples were prepared by sedimentation of suspensions onto glass slides and maintained at constant relative humidity of 47% for 48 h.

The zeta potential determinations were done using the same Brookhaven equipment utilized for Dapp determinations with KCl 10^{-3} M as supporting electrolyte and HCl or NaOH for pH regulation.

Scanning electron microscopy (SEM) micrographs were performed on a Zeiss Supra 40 microscope. Samples were fixed to 10 mm Cu mounts. In addition, energy dispersive spectroscopy (EDS) was carried out using an Oxford X-Max detector to attain the qualitative and semiquantitative composition of the samples.

2.2.3 Adsorption experiments

A stock solution of 0.63 mM was prepared by adding the corresponding amount of NFX to Milli-Q water. Additional concentrations were obtained by dilution in Milli-Q water. In order to evaluate NFX removal efficiency (E%) of all adsorbents, preliminary adsorption experiments were performed in batch conditions at NFX initial concentration of 0.63 mM (8 mL, contact time 24 h, 25 °C, solid/liquid ratio: 1 g L^{-1}) and pH 7.0, at which NFX remains as zwitterion. The removal efficiency was calculated by Eq. (1):

$$E(\%) = \frac{C_o - C_e}{C_o} \times 100\% \quad (1)$$

where: C_o and C_e are the initial and equilibrium NFX concentrations in solution, respectively.

Table 1 Experimental conditions and identification of the products obtained

Initial sample	Acid activation	Thermal treatment	Post- activation	Name
M	–	210 °C, 24 h	–	M-210
M	–	210 °C, 24 h	500 °C, 1 h	M-210-500
D	–	210 °C, 24 h	–	D-210
MD	–	210 °C, 24 h	–	MD-210
MD	ac1	210 °C, 24 h	–	MDac1-210
MD	ac3	210 °C, 24 h	–	MDac3-210
MD	–	210 °C, 24 h	500 °C, 1 h	MD-210-500
MD	ac1	210 °C, 24 h	500 °C, 1 h	MDac1-210-500
MD	ac3	210 °C, 24 h	500 °C, 1 h	MDac3-210-500

On selected adsorbents, adsorption isotherms were performed using a NFX concentration range from 0.003 to 0.63 mM for 24 h at 25 °C, under continuous stirring (200 rpm). After 24 h of equilibrium time, the suspensions were centrifuged at 4000×*g* for 20 min, and the supernatant was isolated by filtration (nitrocellulose membranes of 0.45 µm pore size). After the adsorption process, solids were recovered for further characterizations.

The NFX concentration of adsorption supernatants was determined by high performance liquid chromatography (HPLC), coupled with UV–visible detection, in a Shimadzu HPLC C18 column (4.6 mm × 250 mm, 4.6 µm). The measurements were made at 278 nm, with a 25:75 solution of acetonitrile: phosphate buffer at pH 3 used as mobile phase (Paredes-Laverde et al. 2018), flow rate 0.8 mL min^{-1}, injection volume 10 µL. The retention time was 3.7 min.

The Langmuir isotherm model and Freundlich isotherm equation used to adjust the experimental data are given by Eqs. (2) and (3), respectively.

$$Q = Q_{max} k_L Ce / \left(1 + k_L Ce\right) \quad (2)$$

$$Q = K_f Ce^{(1/n)} \quad (3)$$

In Eq. (2), Q_{max} is the maximum amount adsorbed within a monolayer (mmol g^{-1}) and k_L (L $mmol^{-1}$) is the Langmuir adsorption constant, which is related to the affinity between the adsorbate and adsorbent. The Langmuir isotherm model assumes monolayer adsorption on a surface with a finite number of identical sites, where all sites are energetically equivalent and without interaction between adsorbed molecules.

The Freundlich isotherm equation describes non-ideal and reversible adsorption, not restricted to the formation of a monolayer (Foo and Hameed 2010). At present, this empirical equation is widely applied to multilayer adsorption, with nonuniform distribution of adsorption heat and affinities over a heterogeneous surface (Adamson and Gast 1997). In Eq. (3), K_f [(L $g^{-1})^{1/n}$] is a Freundlich constant, and 1/n (dimensionless number) is a measure of the adsorption intensity (Sanchez-Martin et al. 2006).

2.2.4 Adsorption–desorption cycles

In order to evaluate the reusability, chemical stability and adsorption capacity of the adsorbents, four successive adsorption–desorption cycles of NFX were carried out, in which a new adsorption step was performed after each desorption. The adsorption conditions were the same as indicated previously. Desorption experiments were done following the procedure in previous work (Flores et al. 2017). Briefly, after each adsorption step half the volume of the supernatant (4 mL) was removed and an equal volume of Milli-Q water was added under continuous stirring for another 24 h. In each step the desorbed NFX was determined as indicated for the adsorption process. Then, all the solids of each NFX adsorption–desorption cycle were dried at 60 °C overnight.

3 Results and discussion

Figure 2a–c shows the experimental N_2 adsorption–desorption isotherms for M, MDac3-210 and MDac3-210-500 samples. The last ones are representative of the MD materials obtained.

The M sample exhibited a type IV isotherm according to the IUPAC classification (Sing et al. 1985), with a hysteresis loop type H3, related to materials with plate-like particle aggregates. A quick increase of N_2 adsorbed volume at high relative pressures (near 1) corresponded to N_2 adsorption on larger mesopores or macropores related to voids between particle aggregates, while the smooth adsorption increase at the intermediate relative pressure indicated the presence of mesopores formed by interparticle voids in the sample. The low adsorption at low relative pressure suggested a small contribution of micropores (Roca Jalil et al. 2013).

Similar N_2 adsorption isotherms were found for MD materials with acid treatment and with further thermal activation. The adsorption isotherms of MDac3-210 and MDac3-210-500 samples (Fig. 2b and c, respectively) showed a type V isotherm with hysteresis loops type H1, indicative of weak adsorbate-adsorbent interactions of certain porous materials (Sing et al. 1985).

The specific surface area (S_{N2}), water vapor adsorbed and apparent particle diameter (Dapp) of raw M, D and MD materials are summarized in Table 2.

The hydrothermal treatment of M sample generated a 23% decrease of the initial S_{N2} value assigned to an interlayer collapse, and also to a decrease in the number of micropores with the corresponding increase of mesoporosity (Torres Sánchez et al. 2011).

The low S_{N2} value obtained for D-210 sample was in agreement with those observed for hydrothermal carbons (Kubo et al. 2010; Yao et al. 2014; Zhang et al. 2015; Zhu et al. 2014). The hydrothermal carbon coating on raw M sample caused 80% decrease of the specific surface value (MD-210 sample), which was reverted by further thermal treatment in MD-210-500 sample attaining a value similar to that of M-210 or M-210-500 samples.

The increase of S_{N2} value, for MD samples after 500 °C thermal treatment, with the phosphoric acid concentration increase (63% and 45%, for ac1 and ac3 treatment, respectively) was in agreement with that found for carbons and M submitted to a comparable acid treatment (Puziy et al. 2003; Wang et al. 2010a, 2011), and assigned mainly to a

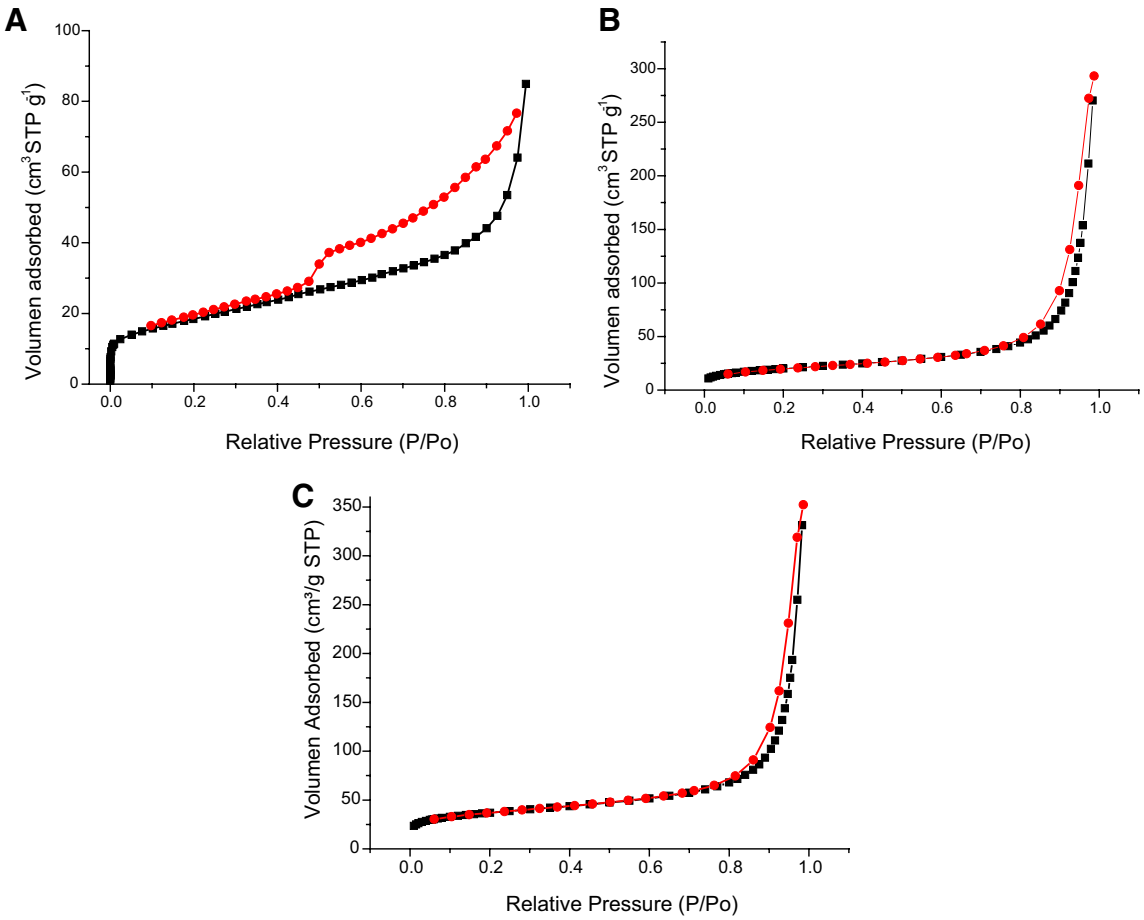

Fig. 2 Experimental N_2 adsorption–desorption isotherms at − 196 °C for: (**a**) M, (**b**) MDac3-210 and (**c**) MDac3-210-500

Table 2 Specific surface (S_{N2}), water vapor adsorbed and apparent particle diameter (Dapp) of indicated samples

Sample	S_{N2} ($m^2\ g^{-1}$)	Water vapor adsorbed ($mg\ g^{-1}$)	Dapp (nm)
M	65.5	101	674 ± 51**
M-210	50.4	111	661 ± 15
M-210-500	54.2*	38	794 ± 24
D-210	12	44	833 ± 13
MD-210	1.2	83	556 ± 9
MD-210-500	50.9	25	510 ± 10
MDac1-210	46.4	44	523 ± 15
MDac3-210	72.1	24	819 ± 17
MDac1-210-500	125.0	39	484 ± 9
MDac3-210-500	131.6	31	730 ± 16

*Data from Torres Sánchez et al. (2011)

**Data from Gamba et al. (2015)

partial destruction of the M sample structure (Jozefaciuk and Bowanko 2002).

The CA determination of M sample indicated a value of 57 ± 2° (Fig. S1A in supplementary information) in agreement with data reported previously (Del Mar Orta et al. 2019; Schampera et al. 2016). When the hydrothermal carbonization step was performed, the CA increased to non-determinable values (see MDac3-210-500 sample in Fig. S1B in supplementary material), pointing out the hydrophility increase attained, in agreement with that previously found for carbon obtained by hydrothermal synthesis (Sun and Li 2004).

The determination of water vapor adsorption for all samples is summarized in Table 2, and used as an approach to M hydrophobicity-hydrophility changes generated by thermal or acid activation on the MD samples. Particularly for M sample, the thermal treatment up to 210 °C decreases the interlayer thickness by loss of H_2O with spontaneous rehydration, whereas dehydroxylation from 350 °C or a higher temperature results from the octahedral hydroxyl exit (Emmerich et al. 2001). These behaviors were reflected in

the almost constant adsorbed water vapor value attained for sample M-210 with respect to M sample, and by the further decrease in the water vapor adsorbed value (37%) found for M-210-500 sample (Table 2).

The samples, with and without M, evidenced a general decrease of water adsorption amount. For MD-210, the adsorbed water vapor value was between those of D-210 and M samples, indicating the coverage of clay surface by HTC.

The water vapor adsorbed for MD materials showed lower values (Table 2) than that of M sample. The 8% decrease and 20% increase for samples with ac1 and ac3 treatment, respectively, could indicate the M greater contribution to vapor water adsorption. As will be seen in the XRD section (Fig. 3), M collapsed in MDac3-210 sample, which could explain the fact that adsorbed water vapor value did not decrease when it was submitted to 500 °C thermal treatment but it does when MDac1-210 is taken to 500 °C.

Table 2 also lists the aggregate sizes measured as Dapp for all samples. The increase of Dapp for M sample with thermal treatment was in line with the specific surface decrease and changes in porosity (Torres Sánchez et al. 2011), and assigned previously to microporous changes associated with the thermal treatment (Fernández et al. 2013). A similar decrease of Dapp values for MD-210, MDac1-210 and MDac3-210 with respect to M sample was found. The further thermal treatment of acid-treated samples (MDac1-210-500 and MDac3-210-500 samples) produced an increase of Dapp value (around 8%) and a decrease for MD210-500 sample, which could be assigned to changes in electrostatic repulsion originated in different surface electrical charges as will be evaluated further in the zeta potential section.

The thermal and/or acid treatments modify the M structure (Torres Sánchez 1997; Wang et al. 2010a), a way of evaluating their consequences is to study the changes that are generated in the basal reflection. Figure 3a–c shows the 001 value for M and its thermally treated products, MD thermally and acid activated, and the last products with further 500 °C treatment, respectively.

The M sample treated at 210 °C did not modify the initial basal space value (at around 1.25 nm), while further treatment at 500 °C shifted the 001 value to 0.98 nm (Fig. 3a), indicative of the interlayer collapse (Torres Sánchez et al. 2011).

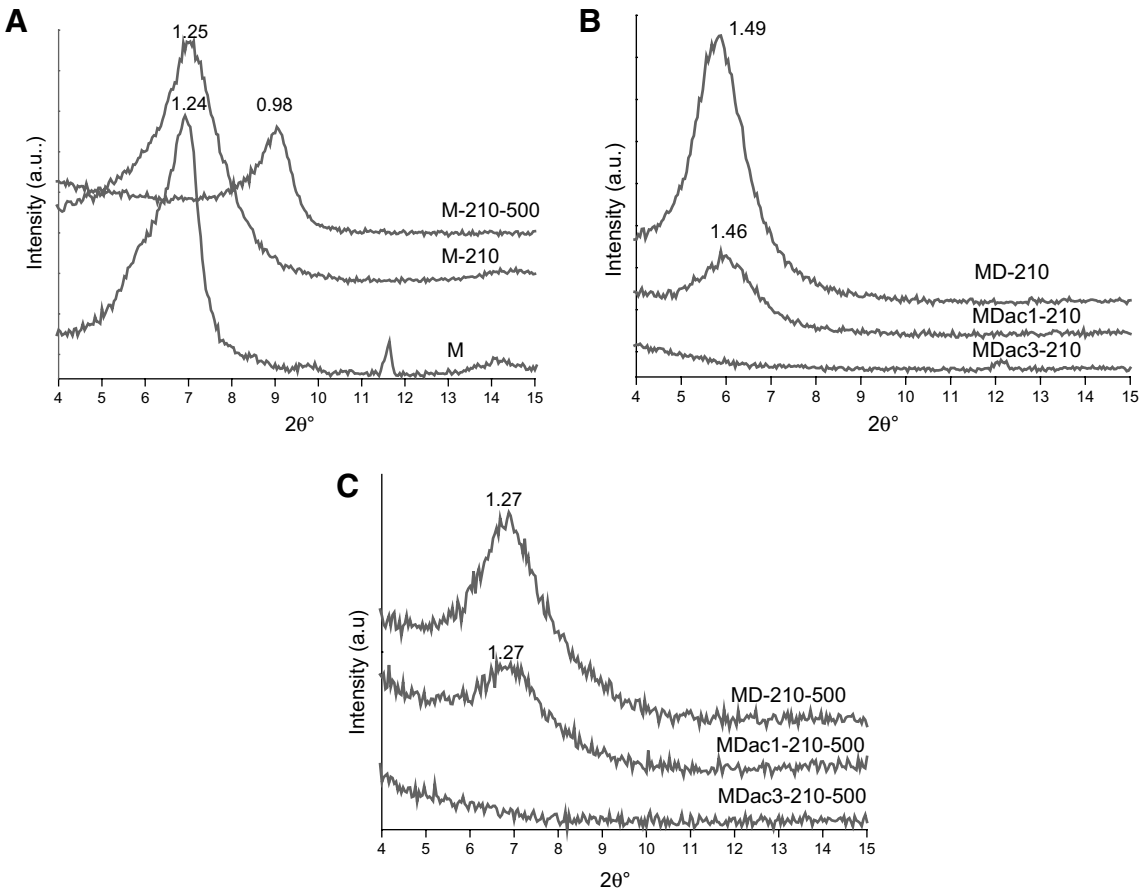

Fig. 3 Partial XRD patterns of: (**a**) M, M-210 and M-210-500; (**b**) MD-210, MDac1-210 and MDac3-210; and (**c**) MD-210-500, MDac1-210-500 and MDac3-210-500 samples. Basal spacing values (d001) are expressed in nm

The dextrose incorporation and further 210 °C treatment (MD-210 sample) produced a 001 value shift of 0.24 nm with respect to those of M-210 sample (Fig. 3b) indicating the entrance of carbon products into the interlayer. For the MD acid-activated samples, besides a similar 001 value shift to that of MD-210 sample, an intensity decrease of the diffraction peaks with the increase of acid concentration is observed, producing, in MDac3-210 sample, the loss of the silicate layer structure sufficiently ordered and oriented to show the basal peak (Wang et al. 2010a).

The further thermal treatment of MD and MD acid-activated samples at 500 °C (Fig. 3c) revealed a constant interlayer thickness decrease of around 0.20 nm, indicative of the carbonization (Puziy et al. 2003) and previous acid amorphization.

In order to elucidate whether the external surface acted as hydrothermal carbon adsorption site, the zeta potential was measured before and after carbon loading (Fig. 4). The zeta potential values give information only about the external surface charge, while the interlayer or inner surface charge remained always neutralized (Bianchi et al. 2013).

The flat curve and pH-independent zeta potential behavior (at around −30 mV) over the entire pH range (from pH 3 to 12) found for M sample (Fig. 4) was previously assigned to a constant surface potential (structural or basal sites) and variable charge (edge sites) (Lombardi et al. 2006).

The zeta potential of M and MD samples was negative in the whole pH range, indicating their negatively charged surfaces. The presence of HTC influenced the zeta potential values by significantly increasing the charges of MD samples with respect to M, which appear to reach a point of zero charge at pH 2. This result is in accordance with previous investigations (Li et al. 2014). The zeta potential values for MDac3-210 sample showed a decrease and an increase of the negative zeta potential value from pH 5

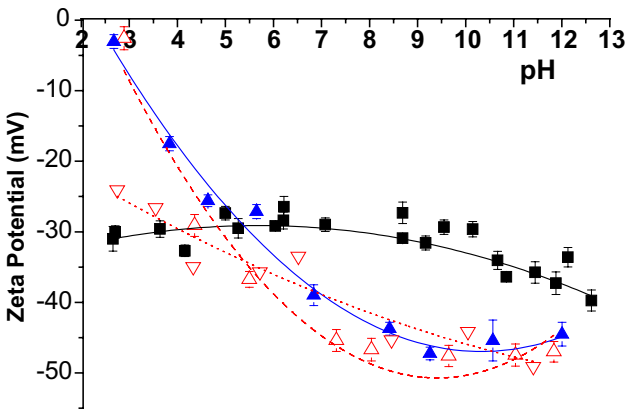

Fig. 4 Zeta potential versus pH for (filled square) M, (downward triangle) MDac1-210, (upward triangle) MDac3-210 and (filled triangle) MDac3-210-500 samples

with respect to that found for M sample. The zeta potential curve for MDac1-210 sample was between that of M and MDac3-210 samples, in agreement with the low acid concentration used with respect to MDac3-210 sample. The MDac3-210-500 sample showed a slight difference towards less negative zeta potential values compared to MDac3-210 sample, as occurred for thermally treated M (see Fig. S2 in supplementary information) and assigned to Al released from the structure producing Al coating of the M surface (Fernández et al. 2013). Consequently, the zeta potential changes of MDac1-210, MDac3-210 and MDac3-210-500 samples were assigned to carbon compounds remaining at the external M surface. The zeta potential values of D-210 and MD-210 samples were also performed, and negatively charged surfaces in all pH range were found (Fig. S3 in supplementary material). These changes in zeta potential values could be responsible for the Dapp value variation evidenced in Table 2.

From the results of Dapp (Table 2) the thermal treatment at 500 °C did not markedly modify the particle size values of samples without this thermal treatment. In order to verify changes in the particle size and morphology produced by the acid treatment, the MD-210-500 and MDac3-210-500 samples were selected to be analyzed by SEM (Fig. 5a and b, respectively). From these figures mean values of 500–600 nm and 700–800 nm were calculated for MD-210-500 and for MDac3-210-500 samples, respectively. These results were similar to the Dapp values obtained previously for these samples (Table 2).

Clay particles exhibit a more irregular surface in MDac3-210-500 sample (Fig. 5b) than in MD-210-500 sample (Fig. 5a), evidencing the acid treatment attack on the clay structure, as was also pointed out by the interlayer collapse observed by XRD (Fig. 3).

The chemical composition results of the MD materials investigated by EDS are summarized in Table 3. Higher carbon content was found for the samples without acid activation (MD-210 and MD-210-500) compared to those treated with acid (MDac3-210 and MDac3-210-500). This behavior could be assigned to the formation of soluble organic molecules (Jin and Enomoto 2010) during the carbonization process in the presence of acid, which were removed with the later washing step.

In addition, a complete release of interlayer cations (Na^+, Ca^{2+}, and K^+ ions) was observed after the hydrothermal treatment for acid-activated samples (Table 3), validating the clay structure modification found by XRD.

The carbon coverage of montmorillonite by hydrothermal treatment was evidenced by the decrease of the structural elements (Si, Al, Mg and Fe) (Barraqué et al. 2018).

In order to compare the NFX adsorption efficiency for all samples, pH 7 and $C_o = 0.63$ mM were chosen to attain neutral and soluble NFX, and the results are shown in Fig. 6.

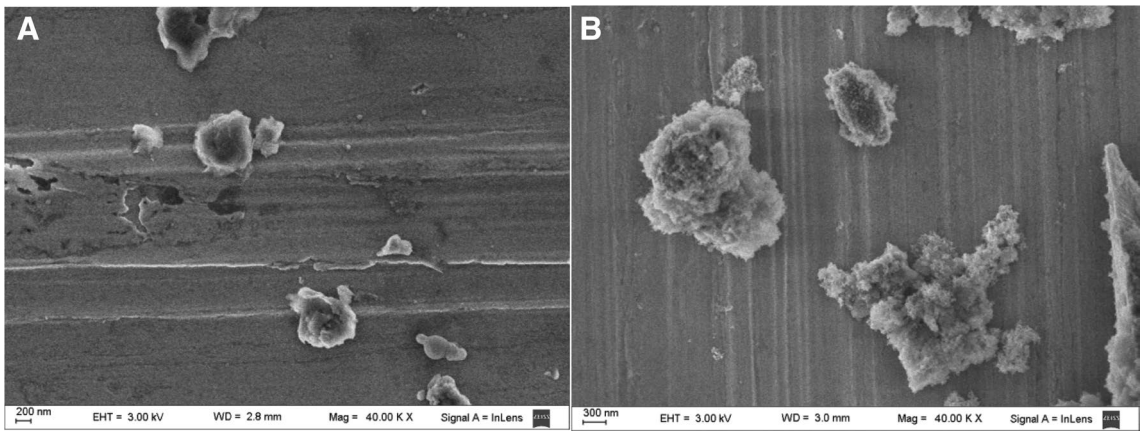

Fig. 5 SEM micrograph of MD-210-500 (**a**) and MDac3-210-500 (**b**) samples

Table 3 EDS results of indicated samples

Samples	C (%)	Na_2O (%)	MgO (%)	Al_2O_3 (%)	SiO_2 (%)	P_2O_5 (%)	K_2O (%)	CaO (%)	TiO (%)	Fe_2O_3 (%)
MD-210	45.3	0.2	1.8	11.9	37.1	0.1	0.1	0.7	0.2	2.5
MD-210-500	41.8	0.3	1.8	12.4	39.0	–	0.1	0.6	0.7	3.2
MDac3-210	29.4	–	0.4	11.4	32.9	23.1	–	–	0.4	2.3
MDac3-210-500	28.7	–	0.6	7.1	43.3	15.8	–	–	0.3	4.1

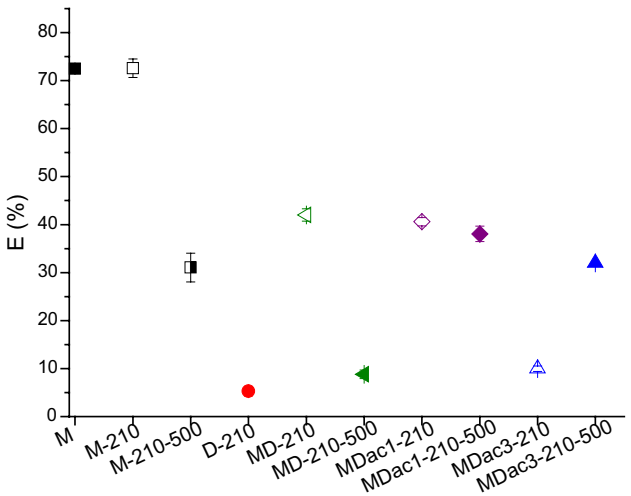

Fig. 6 NFX removal efficiency for the indicated samples at pH 7, solid/liquid ratio 1 g L^{-1} and C_0 = (0.63 mM NFX)

The M sample attained the highest adsorption efficiency (around 73%) among all evaluated samples, despite the higher specific surface area obtained for MD acid and thermally treated samples (MDac1-210-500 and MDac3-210-500). For M-210-500 sample a 17% decrease in surface area (Table 2) and a 57% decrease in adsorption efficiency with respect to M were observed. Both could be assigned to the interlayer collapse and loss of negative charges evidenced by XRD and zeta potential measurements, respectively (Fig. 3, and Fig. S2 in supplementary information). However, an opposite effect was found for MD-210 and MD-210-500 samples, decreasing E% with the increase of S_{N2} values, revealing the importance of the M structure in the adsorption. This effect is corroborated with the low E% of D-210. The M groups Si–O–Si, O–H could interact with the NFX molecule through electrostatic attraction as H-bond and also π–π bond (Li et al. 2017).

The MD materials reached lower E% values (around 30%) than those of M and M-210 samples, despite the increase in S_{N2} values of the former. In D-210 and in the samples where the M structure was lost due to thermal or acid treatment (M-210-500, MD-210-500, MDac1-210-500, MDac3-210 and MDac3-210-500 samples), the effect that would most influence the adsorption process seemed to be the filling of the pores, so the increase of S_{N2} would be responsible for the adsorption increase (Fig. 6) (E% from 5.30 to 32.02, corresponding to D-210 and MDac3-210-500 samples, respectively).

The NFX adsorption on different carbon species showed different Q_{max} values, i.e., for activated carbon and carbon nanotubes 0.35 and 0.17–0.24 mmol g^{-1}, respectively, which were assigned mainly to the different specific surface areas of 664 and 117–228 m^2 g^{-1}, respectively (Wang et al. 2010b), the hydrogen bonds being proposed as a mechanism

for understanding the sorption of aromatics on activated carbon (Ahnert et al. 2009). While for Trapa natans husk activated carbon (TAC), with a large surface area of 1274 m^2 g^{-1} and mesoporous structure, a Q_{max} of 2 mmol g^{-1} was attained, and carboxylic and hydroxyl groups were indicated as contributing to the sorption of NFX, electrostatic-hydrophobic interactions were proposed to be the principal NFX sorption mechanism (Xie et al. 2011).

The differences found in Q_{max} for carbon species, discussed above, and the possible technological application of these MD samples as retention columns, made it necessary to determine, as a first step, the NFX adsorption in a range of concentration.

From Fig. 6 samples MD-210 and MDac3-210-500 were chosen to obtain information about their adsorption capacity to remove NFX in a concentration range from 3 10^{-3} to 0.63 mM. The MD-210 sample was selected because it attained the highest E% value among the hybrid materials, and MDac3-210-500 sample as representative of the MD samples with high specific surface and similar E% value to that of MD-210 sample. To compare the adsorbent efficiency, NFX adsorption isotherms were performed, and experimental points were fitted to Langmuir and Freundlich isotherm expressions.

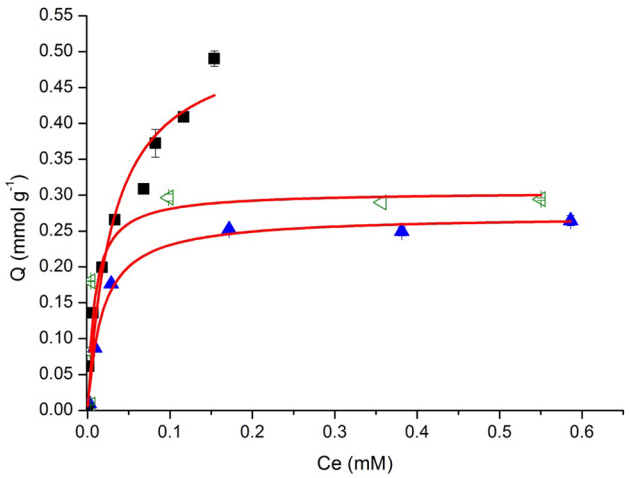

Fig. 7 NFX adsorption isotherm for: (filled square) M; (left pointing triangle) MD-210 and (filled triangle) MDac3-210-500 samples. Lines were obtained from Eq. (2) using the Langmuir model

As was indicated before by the removal efficiency (Fig. 6), sample M showed the highest adsorption capacity, attaining a Q_{max} of 0.53 mmol g^{-1}, while 0.30 and 0.27 mmol g^{-1} were attained for MD-210 and MDac3-210-500 samples, respectively (Fig. 7; Table 4). This behavior seemed to indicate that the M surface sites were preferred for NFX adsorption.

The solid lines in Fig. 7 represent the Langmuir model applied to the adsorption of NFX, and the calculated lines and experimental data match well with the values of the regression coefficient (R^2) within 0.75 and 0.99 (Table 4).

The higher Langmuir regression coefficient values obtained for MD-210 and MDac3-210-500 samples (0.75 and 0.99, respectively) than those obtained for Freundlich equation (Table 4) showed their best fit to the experimental data, indicating that the Langmuir assumptions (monolayer adsorption on homogeneous surface sites) were accomplished. The better fit of the Langmuir equation than the Freundlich one was assigned to the preferential NFX adsorption at the M homogenous surface sites than at the heterogeneous surface sites of carbon/montmorillonite hybrids decreasing the Q_{max} attained for these samples. The same better correlation to Langmuir than to Freundlich expressions was found previously (Li et al. 2017), using clay-biochar composite (from potato stem and natural attapulgite) as NFX adsorbent, and achieving a Q_{max} (0.009 mmol g^{-1}) lower than those found in this work for MD-210 and MDac3-210-500 samples.

The affinity between adsorbent and adsorbate, represented by the constant K_L, indicated that despite the decrease of Q_{max} for MD-210 and MDac3-210-500 with respect to M sample, the K_L value increased, evidencing a better affinity of these adsorbents for NFX than M sample.

The affinity constant (K_L) of the products for the adsorbate could allow them to be used in the NFX concentration range found in wastewater treatment plants (i.e., 1.3 10^{-6} and 0.02 10^{-3} mM in USA (Fu et al. 2017) and in China (Bu et al. 2013), respectively).

The M, MD-210 and MDac3-210-500 samples with NFX maximal adsorption were used to determine the NFX adsorption at the M inner and outer surface sites. To achieve this goal, the XRD shift of the M basal space (d 001) was used to evidence changes produced at the interlayer space thickness in order to determine the entrance or not of NFX into the M inner surface. Besides, changes of zeta potential

Table 4 Parameters of the Langmuir and Freundlich expressions fitted to the experimental adsorption data

Samples	Langmuir			Freundlich		
	Q_{max} (mmol g^{-1})	k_L (L $mmol^{-1}$)	R^2	K_f (L $g^{-1})^{1/n}$	1/n	R^2
M	0.53 ± 0.05	32 ± 10	0.95	1.06 ± 0.09	0.43 ± 0.03	0.98
MD-210	0.30 ± 0.04	118 ± 73	0.75	0.37 ± 0.08	0.22 ± 0.09	0.64
MDac3-210-500	0.27 ± 0.01	563 ± 83	0.99	0.33 ± 0.05	0.26 ± 0.07	0.83

values were employed to prove modifications of the M outer surface charge. The d 001 and zeta potential values of samples with and without NFX were determined and are listed in Table 5.

The presence of NFX in M sample produced an interlayer thickness increase of 0.42 nm. Taking into account that the interlayer water release leads to an interlayer thickness value of 0.96 nm (Emmerich 2000), the interlayer increase by NFX entrance was 0.70 nm, a value that is close to the maximum z length of NFX: 0.66 nm (Yang et al. 2012). This could indicate that NFX enters the M interlayer due to the benzene capacity to adopt the shape of a flat hexagon along with its derivatives (Pirani et al. 2001), and because of the zwitterion NFX property at the adsorption pH, at this inner surface the adsorption mechanism may be a cation exchange. For MD-210 sample, the presence of carbon at the interlayer was indicated previously (due to the 0.25 nm interlayer thickness increase), while the further NFX occurrence at the interlayer could not be evidenced by the low shift of d 001 value (0.05 nm, Table 5).

For MDac3-210-500 sample, due to the interlayer collapse the effect of NFX on this surface could not be determined.

The zeta potential values after NFX adsorption evidenced an increase (of around 6 mV), no change, and a decrease (of around 24 mV) of the negative electrical charge for M, MD210 and MDac3-210-500 samples, respectively. For M sample these shifts of zeta potential values suggest an electrostatic attraction mechanism between the NFX protonated amine group ($-NH_2^+$) and the negatively charged outer solid surface. In MD-210 sample, the coverage of M outer surface by carbon, while a negative electric charge similar to that of M remained (Fig. S3 in supplementary material), could reduce the number of sites of the solid external surface for NFX adsorption, and NFX adsorption could happen mainly at the inner surface (interlayer) where the thickness was already increased by the income of carbon shielding. For MDac3-210-500 sample, the zeta potential changes with respect to M samples were assigned to carbon compounds remaining at the outer M surface furthermore, this sample showed the highest affinity for NFX among the evaluated adsorbents. In this case a π–π electron donor–acceptor (EDA) interaction could be considered as one of the predominant driving forces for NFX adsorption (Wang et al. 2010b). Particularly, at a neutral pH, the benzene ring on NFX can function as a π-electron acceptor due to the strong electron-withdrawing ability of the fluorine group, decreasing the zeta potential values.

The different interaction mechanisms on the surface of the materials studied will be better evaluated by NFX adsorption at different pH values to be performed in future work.

In order to evaluate the capacity of the studied materials to be reused as NFX adsorbents and consequently, their technological applicability, NFX adsorption–desorption cycles were performed. As can be seen in Fig. 8, along the cycles the NFX adsorbed amount decreased for all samples. The NFX desorbed amount was ≤ 7% with respect to the total NFX adsorbed, increasing for all the materials until cycle 3, being slightly low particularly for MD samples at the fourth cycle.

Although M sample showed the best E% among the samples evaluated, it also presented the highest loss of adsorption capacity (around 98%) within the cycles performed. For the MD materials two different behaviors were found. For the MD-210 sample, a similar behavior to that of sample M was found with a loss of total adsorption capacity of around 96% within the cycles carried out. While for the MDac3-210-500 sample, a greater conservation of the adsorption

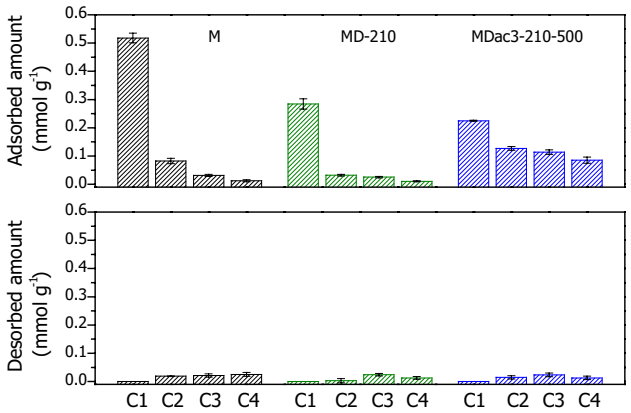

Fig. 8 Adsorbed and desorbed NFX amount obtained after each adsorption–desorption cycle for: (columns group at left) M, (columns group at middle) MD-210 and (columns group at right) MDac3-210-500 samples. *C1*, *C2*, *C3* and *C4* means: 1, 2, 3 and 4 cycles, respectively

Table 5 d001 and zeta potential values for indicated samples

Sample	Without NFX			With NFX		
	pH	d 001 (nm)	Zeta potential (mV)	pH	d 001 (nm)	Zeta potential (mV)
M	7.0	1.24	−29 ± 1	6.9	1.66	−35 ± 1
MD-210	7.5	1.49	−34.0 ± 0.9	7.4	1.54	−33.7 ± 0.8
MDac3-210-500	7.3	n.d.	−39.70 ± 0.04	7.3	nd	−15.82 ± 0.52

nd Not determined

capacity was observed, with a 64% loss of the total adsorption capacity throughout the cycles.

In general for all samples, the NFX desorbed amount was lower than that adsorbed in each cycle, until cycle 4. Particularly, in cycle 4 the M sample presented the highest NFX desorbed amount with respect to that previously adsorbed in the same cycle (Fig. 8). For MD-210 sample in cycles 3 and 4 the NFX adsorbed was also almost fully desorbed. While the sample MDac3-210-500, presented the highest NFX retention in all cycles among the samples studied.

This different NFX retention behavior, during the adsorption/desorption cycles carried out, could indicate that while for samples M and MD-210 the saturation of the surface sites by NFX was reached, in the sample MDac3- 210-500 it was not like that. This result points out sample MDac3-210-500 as the best material, among the samples evaluated, for technological reuse in the adsorption of NFX.

4 Conclusions

The hybrid materials were obtained efficiently. The hydrothermal carbon was incorporated both in the surface and in the interlayer of M. The activation methods used to increase S_{N2} of the MD materials were satisfactory, reaching specific surface values greater than M. Although none of the MD materials achieved an adsorption higher than M, all were efficient in NFX removal. However, the results attained from adsorption–desorption cycles, the highest value of K_L obtained for MDac3-210-500 sample, and taking into account the low environmental concentrations of NFX, could suggest this material as better NFX adsorbent for successive adsorptions than M sample. In addition, due to the entry of carbon products into the M interlayer, the MD materials could inhibit the initial swelling property of M, providing the advantage of its use as column filler.

Acknowledgements Financial support of the Argentine Ministry of Science, Grant BID-PICT 2014/585, is gratefully acknowledged. M.E.Z.S., F.B. and M.F. acknowledge CONICET fellowships, and M.A.F and R.M.T.S. the National Council of Scientific and Technological Research (CONICET).

References

Adamson, A.W., Gast, A.P.: Physical chemistry of surfaces. Wiley, New York (1997)

Ahnert, F., Pinto, N.G., Arafat, H.A.: A study of the influence of hydrophobicity of activated carbon on the adsorption equilibrium of aromatics in non-aqueous media. Adsorption. **43**, 3421–3429 (2009)

Ai, L., Li, L.: Efficient removal of organic dyes from aqueous solution with ecofriendly biomass-derived carbon@montmorillonite nanocomposites by one-step hydrothermal process. Chem. Eng. J. J. **223**, 688–695 (2013)

Ania, C.O., Pelayo, J.G., Bandosz, T.J.: Reactive adsorption of penicillin on activated carbons. Adsorption. **17**, 421–429 (2011)

Barraqué, F., Montes, M.L., Fernández, M.A., Mercader, R.C., Candal, R.J., Torres, R.M.: Synthesis and characterization of magnetic-montmorillonite and magnetic- organo-montmorillonite: surface sites involved on cobalt sorption. J. Magn. Magn. Mater. **466**, 376–384 (2018)

Bhattacharyya, K.G., Gupta, S.: Sen: adsorption of a few heavy metals on natural and modified kaolinite and montmorillonite: a review. Adv. Colloid Interface Sci. **140**, 114–131 (2008)

Bianchi, A.E., Fernández, M., Pantanetti, M., Viña, R., Torriani, I., Sánchez, R.M.T., Punte, G.: ODTMA + and HDTMA + organo-montmorillonites characterization: new insight by WAXS, SAXS and surface charge. Appl. Clay Sci. **83–84**, 280–285 (2013)

Bu, Q., Wang, B., Huang, J., Deng, S., Yu, G.: Pharmaceuticals and personal care products in the aquatic environment in China: a review. J. Hazard. Mater. **262**, 189–211 (2013)

Del Mar Orta, M., Flores, F.M., Morantes, C.F., Curutchet, G., Torres Sánchez, R.M.: Interrelations of structure, electric surface charge, and hydrophobicity of organo-mica and -montmorillonite, tailored with quaternary or primary amine cations. Preliminary study of pyrimethanil adsorption. Mater. Chem. Phys. **223**, 325–335 (2019)

Emmerich, K.: Spontaneous rehydroxylation of a dehydroxylated CIS-vacant montmorillonite. Clays Clay Miner. **48**, 405–408 (2000)

Emmerich, K., Plötze, M., Kahr, G.: Reversible collapse and Mg2 + release of de- and rehydroxylated homoionic cis-vacant montmorillonites. Appl. Clay Sci. **19**, 143–154 (2001)

Fernández, M., Alba, M.D., Torres Sánchez, R.M.: Effects of thermal and mechanical treatments on montmorillonite homoionized with mono- and polyvalent cations: insight into the surface and structural changes. Colloids Surf. A **423**, 1–10 (2013)

Flores, F.M., Undabeytia, T., Morillo, E., Sánchez, R.M.T.: Technological applications of organo-montmorillonites in the removal of pyrimethanil from water: adsorption/desorption and flocculation studies. Environ. Sci. Pollut. Res. **24**, 14463–14476 (2017)

Foo, K.Y., Hameed, B.H.: Insights into the modeling of adsorption isotherm systems. Chem. Eng. J. **156**, 2–10 (2010)

Fu, H., Li, X., Wang, J., Lin, P., Chen, C., Zhang, X., Suffet, I.H.: Activated carbon adsorption of quinolone antibiotics in water: performance, mechanism, and modeling. J. Environ. Sci. (China) **56**, 145–152 (2017)

Gamba, M., Flores, F.M., Madejová, J., Sánchez, R.M.T.: Comparison of imazalil removal onto montmorillonite and nanomontmorillonite and adsorption surface sites involved: an approach for agricultural wastewater treatment. Ind. Eng. Chem. Res. **54**, 1529–1538 (2015)

Gamba, M., Kovář, P., Pospíšil, M., Torres Sánchez, R.M.: Insight into thiabendazole interaction with montmorillonite and organically modified montmorillonites. Appl. Clay Sci. **137**, 59–68 (2017)

Jin, F., Enomoto, H.: Rapid and highly selective conversion of biomass into value-added products in hydrothermal conditions: chemistry of acid/base-catalysed and oxidation reactions. Energy Environ. Sci. **4**, 382–397 (2010)

Jozefaciuk, G., Bowanko, G.: Effect of acid and alkali treatments on surface - charge properties of selected minerals. Clays Clay Miner. **50**, 771–783 (2002)

Kerkez-Kuyumcu, Ö., Bayazit, Ş.S., Salam, M.A.: Antibiotic amoxicillin removal from aqueous solution using magnetically modified graphene nanoplatelets. J. Ind. Eng. Chem. **36**, 198–205 (2016)

Kubo, S., Demir-Cakan, R., Zhao, L., White, R.J., Titirici, M.M.: Porous carbohydrate-based materials via hard templating. Chemsuschem **3**, 188–194 (2010)

Li, T., Shen, J., Huang, S., Li, N., Ye, M.: Hydrothermal carbonization synthesis of a novel montmorillonite supported carbon nanosphere adsorbent for removal of Cr(VI) from waste water. Appl. Clay Sci. **93–94**, 48–55 (2014)

Li, Y., Wang, Z., Xie, X., Zhu, J., Li, R., Qin, T.: Removal of Norfloxacin from aqueous solution by clay-biochar composite prepared from potato stem and natural attapulgite. Colloids Surf. A **514**, 126–136 (2017)

Lin, S.H., Juang, R.S., Wang, Y.H.: Adsorption of acid dye from water onto pristine and acid-activated clays in fixed beds. J. Hazard. Mater. **113**, 195–200 (2004)

Liu, W., Zhang, J., Zhang, C., Ren, L.: Sorption of norfloxacin by lotus stalk-based activated carbon and iron-doped activated alumina: mechanisms, isotherms and kinetics. Chem. Eng. J. **171**, 431–438 (2011)

Loh, G.O.K., Tan, Y.T.F., Peh, K.K.: Hydrophilic polymer solubilization on norfloxacin solubility in preparation of solid dispersion. Powder Technol. **256**, 462–469 (2014)

Lombardi, B.M., Torres Sanchez, R.M., Eloy, P., Genet, M.: Interaction of thiabendazole and benzimidazole with montmorillonite. Appl. Clay Sci. **33**, 59–65 (2006)

Low, P.F.: The swelling of clay: II. Montmorillonites. Soil Sci. Soc. Am. **46**, 667–676 (1980)

Makowski, P., Demir Cakan, R., Antonietti, M., Goettmann, F., Titirici, M.M.: Selective partial hydrogenation of hydroxy aromatic derivatives with palladium nanoparticles supported on hydrophilic carbon. Chem. Commun. **8**, 999–1001 (2008)

Martínez-Alcalá, I., Guillén-Navarro, J.M., Fernéndez-López, C.: Pharmaceutical biological degradation, sorption and mass balance determination in a conventional activated-sludge wastewater treatment plant from Murcia. Spain. Chem. Eng. J. **316**, 332–340 (2017)

Metya, A., Ghose, D., Ray, N.R.: Development of hydrophobicity of mica surfaces by ion beam sputtering. Appl. Surf. Sci. **293**, 18–23 (2014)

Mochidzuki, K., Sato, N., Sakoda, A.: Production and characterization of carbonaceous adsorbents from biomass wastes by aqueous phase carbonization. Adsorption. **11**, 669–673 (2005)

Özcan, A., Atılır Özcan, A., Demirci, Y.: Evaluation of mineralization kinetics and pathway of norfloxacin removal from water by electro-Fenton treatment. Chem. Eng. J. **304**, 518–526 (2016)

Pacuła, A., Bielańska, E., Gaweł, A., Bahranowski, K., Serwicka, E.M.: Textural effects in powdered montmorillonite induced by freeze-drying and ultrasound pretreatment. Appl. Clay Sci. **32**, 64–72 (2006)

Paredes-Laverde, M., Silva-Agredo, J., Torres-Palma, R.A.: Removal of norfloxacin in deionized, municipal water and urine using rice (*Oryza sativa*) and coffee (*Coffea arabica*) husk wastes as natural adsorbents. J. Environ. Manag. **213**, 98–108 (2018)

Pei, Z., Kong, J., Shan, X.Q., Wen, B.: Sorption of aromatic hydrocarbons onto montmorillonite as affected by norfloxacin. J. Hazard. Mater. **203–204**, 137–144 (2012)

Peng, K., Yang, H.: Carbon hybridized montmorillonite nanosheets: preparation, structural evolution and enhanced adsorption performance. Chem. Commun. **53**, 6085–6088 (2017)

Pirani, F., Cappelletti, D., Bartolomei, M., Aquilanti, V., Scotoni, M., Vescovi, M., Ascenzi, D., Bassi, D.: Orientation of benzene in supersonic expansions, probed by IR-laser absorption and by molecular beam scattering. Phys. Rev. Lett. **86**, 5035–5038 (2001)

Puziy, A.M., Poddubnaya, O.I., Martínez-Alonso, A., Suárez-García, F., Tascón, J.M.D.: Synthetic carbons activated with phosphoric acid III. Carbons prepared in air. Carbon **41**, 1181–1191 (2003)

Rasband, W.S.: ImageJ. US National Institutes of Health, Bethesda, MD (1997)

Roca Jalil, M.E., Vieira, R.S., Azevedo, D., Baschini, M., Sapag, K.: Improvement in the adsorption of thiabendazole by using aluminum pillared clays. Appl. Clay Sci. **71**, 55–63 (2013)

Ross, L., Riley, M.: Solubilities of some variously quinolone antimicrobials substituted. Int. J. Pharm. **63**, 237–250 (1990)

Sanchez-Martin, M.J., Rodriguez-Cruz, M.S., Andrades, M.S., Sanchez-Camazano, M.: Efficiency of different clay minerals modified with a cationic surfactant in the adsorption of pesticides: influence of clay type and pesticide hydrophobicity. Appl. Clay Sci. **31**, 216–228 (2006)

Schampera, B., Tunega, D., Šolc, R., Woche, S.K., Mikutta, R., Wirth, R., Dultz, S., Guggenberger, G.: External surface structure of organoclays analyzed by transmission electron microscopy and X-ray photoelectron spectroscopy in combination with molecular dynamics simulations. J. Colloid Interface Sci. **478**, 188–200 (2016)

Sing, K.S.W., Everett, D.H., Haul, R.A.W., Moscou, L., Pierotti, R.S., Rouquerol, J., Siemieniewska, T.: Reporting physisorption data for gas/solid systems with special reference to the determination of surface area and porosity. Pure Appl. Chem. **57**, 603–619 (1985)

Skubiszewska-Zięba, J., Sydorchuk, V.V., Gun'ko, V.M., Leboda, R.: Hydrothermal modification of carbon adsorbents. Adsorption. **17**, 919–927 (2011)

Stalder, A.F., Melchior, T., Müller, M., Sage, D., Blu, T., Unser, M.: Low-bond axisymmetric drop shape analysis for surface tension and contact angle measurements of sessile drops. Colloids Surf. A **364**, 72–81 (2010)

Sturini, M., Speltini, A., Maraschi, F., Profumo, A., Pretali, L., Irastorza, E.A., Fasani, E., Albini, A.: Photolytic and photocatalytic degradation of fluoroquinolones in untreated river water under natural sunlight. Appl. Catal. B **119–120**, 32–39 (2012)

Sun, X., Li, Y.: Colloidal carbon spheres and their core/shell structures with noble-metal nanoparticles. Angew. Chem. **116**, 607–611 (2004)

Torres Sánchez, R.M.: Mechanochemical effects on physicochemical parameters of homoionic smectite. Colloids Surf. A **127**, 135–140 (1997)

Torres Sánchez, R.M., Genet, M.J., Gaigneaux, E.M., dos Santos Afonso, M., Yunes, S.: Benzimidazole adsorption on the external and interlayer surfaces of raw and treated montmorillonite. Appl. Clay Sci. **53**, 366–373 (2011)

Wang, T.H., Liu, T.Y., Wu, D.C., Li, M.H., Chen, J.R., Teng, S.P.: Performance of phosphoric acid activated montmorillonite as buffer materials for radioactive waste repository. J. Hazard. Mater. **173**, 335–342 (2010a)

Wang, Z., Pan, B., Xing, B.: Norfloxacin sorption and its thermodynamics on surface modified carbon nanotubes. Environ. Sci. Technol. **44**, 978–984 (2010b)

Wang, L., Guo, Y., Zou, B., Rong, C., Ma, X., Qu, Y., Li, Y., Wang, Z.: High surface area porous carbons prepared from hydrochars by phosphoric acid activation. Bioresour. Technol. **102**, 1947–1950 (2011)

Wu, X., Zhu, W., Zhang, X., Chen, T., Frost, R.L.: Catalytic deposition of nanocarbon onto palygorskite and its adsorption of phenol. Appl. Clay Sci. **52**, 400–406 (2011)

Xie, H., Liu, W., Zhang, J., Zhang, C., Ren, L.: Sorption of norfloxacin from aqueous solutions by activated carbon developed from Trapa natans husk. Sci. China Chem. **54**, 835–843 (2011)

Yan, B., Niu, C.H., Wang, J.: Kinetics, electron-donor-acceptor interactions, and site energy distribution analyses of norfloxacin adsorption on pretreated barley straw. Chem. Eng. J. **330**, 1211–1221 (2017)

Yang, W., Lu, Y., Zheng, F., Xue, X., Li, N., Liu, D.: Adsorption behavior and mechanisms of norfloxacin onto porous resins and carbon nanotube. Chem. Eng. J. **179**, 112–118 (2012)

Yao, Y., Gao, B., Fang, J., Zhang, M., Chen, H., Zhou, Y., Creamer, A.E., Sun, Y., Yang, L.: Characterization and environmental applications of clay-biochar composites. Chem. Eng. J. **242**, 136–143 (2014)

Zeiler, H.-J., Förster, D., Beermann, D., Wingender, W., Schacht, P.: Bactericidal activity of ciprofloxacin, norfloxacin and ofloxacin in serum and urine after oral administration to healthy volunteers. Infection **16**, S19–S23 (1988)

Zhang, R., Chen, C., Li, J., Wang, X.: Preparation of montmorillonite@carbon composite and its application for U(VI) removal from aqueous solution. Appl. Surf. Sci. **349**, 129–137 (2015)

Zhu, X., Liu, Y., Zhou, C., Luo, G., Zhang, S., Chen, J.: A novel porous carbon derived from hydrothermal carbon for efficient adsorption of tetracycline. Carbon **77**, 627–636 (2014)

Zorita, S., Mårtensson, L., Mathiasson, L.: Occurrence and removal of pharmaceuticals in a municipal sewage treatment system in the south of Sweden. Sci. Total Environ. **407**, 2760–2770 (2009)